The Astrophysical Journal, 945:168 (10pp), 2023 March 10 https://doi.org/10.3847/1538-4357/acb929
© 2023. The Author(s). Published by the American Astronomical Society.
OPEN ACCESS

Low-frequency Waves Due to Newborn Interstellar Pickup Ions Observed from 43 to 47 au by the Voyager 1 Spacecraft

Lily A. Ercoline[1,2,3], Charles W. Smith[1,4], Matthew R. Argall[1,4], Colin J. Joyce[1,4], Philip A. Isenberg[1,4], Bernard J. Vasquez[1,4], Nathan A. Schwadron[1,4], Justyna M. Sokół[5], and Leonard F. Burlaga[1,6]
[1] Physics Department and Space Science Center, Morse Hall, University of New Hampshire, Durham, New Hampshire, USA; LilyErcoline@gmail.com, Matthew.Argall@unh.edu
[2] Contoocook Valley Regional High School, Peterborough, New Hampshire, USA
[3] Bennington College, Bennington, Vermont, USA
[4] University of New Hampshire, Durham, New Hampshire, USA; Charles.Smith@unh.edu, Colin.Joyce@unh.edu, Phil.Isenberg@unh.edu, Bernie.Vasquez@unh.edu, Nathan.Schwadron@unh.edu
[5] Southwest Research Institute, San Antonio, Texas, USA; justyna.sokol@swri.org
[6] Leonard F Burlaga, Inc., Davidsonville, Maryland, USA; lburlagahsp@verizon.net
Received 2022 September 30; revised 2023 January 31; accepted 2023 February 3; published 2023 March 20

Abstract

Interstellar neutral atoms enter the heliosphere at a relatively slow speed corresponding to the motion of the Sun through the local interstellar medium, which is approximately 25 km s^{-1}. Neutral hydrogen atoms enter from the approximate location of the Voyager spacecraft and are eventually ionized primarily by collision with thermal solar wind ions. An earlier analysis by Hollick et al. examined low-frequency magnetic waves observed by the Voyager spacecraft from launch through 1990 that are thought to arise from the scattering of newborn interstellar pickup H^+ and He^+. We report an analysis of Voyager 1 observations in 1991, which is the last year of high-resolution magnetic field data that are publicly available, and find 70 examples of low-frequency waves with the characteristics that suggest excitation by pickup H^+ and 10 examples of waves consistent with excitation by pickup He^+. We find a particularly dense cluster of observations at the tail end of what is thought to be a Merged Interaction Region (MIR) that was previously studied by Burlaga & Ness using Voyager 2 observations. This is not unexpected if the MIR is followed by a large rarefaction region, as they tend to be regions of reduced turbulence levels that permit the growth of the waves over the long time periods that are generally required of this instability.

Unified Astronomy Thesaurus concepts: Pickup ions (1239); Solar wind (1534); Interplanetary turbulence (830); Interplanetary magnetic fields (824)

1. Introduction

Pickup ion (PUI) populations are formed when neutral atoms are ionized by any of several methods to produce an electrically charged particle. The neutral atoms are often, although not always, considered to be low-energy particles in the frame of the Sun when dealing with PUIs in the solar wind. However, the particle is moving through the solar wind at approximately the solar wind speed, such that when ionized it becomes a suprathermal ion with energy significantly greater than the thermal speed of the background population. This often results in suprathermal ion populations in regions of space that an ion of that energy would not normally be able to reach in the numbers seen. The resulting suprathermal ion population is unstable and excites magnetic waves as they scatter. A key feature of these waves is that they are seen at spacecraft-frame frequencies equal to or greater than the ion cyclotron frequency of that ion species ($f_{sc} \geqslant f_{i,c}$), where $f_{i,c} \equiv eB_0(2\pi m_i c)^{-1}$, e is the electrical charge of the ion, B_0 is the mean magnetic field strength, m_i is the mass of the ion, and c is the speed of light. For protons (pickup H^+), which are the primary focus of this paper, $f_{p,c} = 0.0152B_0$, where B_0 is measured in nanoTesla (nT) and $f_{p,c}$ is in Hz. The instabilities are weak and seldom result in an observable enhancement of magnetic power at these frequencies. The waves are most readily identified by significant changes in the magnetic fluctuation polarization spectra at these frequencies. Normal background spectra of the solar wind magnetic field are unpolarized at $f_{sc} \simeq f_{p,c}$.

The earliest observations of waves excited by newborn interstellar pickup ions were reported by Murphy et al. (1995) using Ulysses data following the Jovian encounter. More recent studies using Voyager data have shown that Jupiter is an abundant source of newborn pickup H^+ that produce waves when the interstellar source is insufficient (Hollick et al. 2022). Additional studies using ACE, Ulysses, and Voyager data have revealed an abundance of waves from 1 to 44 au arising from newborn interstellar PUI H^+ and He^+ whenever the turbulence is sufficiently weak as to allow for the growth of the waves over the long times required of the relatively weak instability (Joyce et al. 2010; Cannon et al. 2013, 2014a, 2014b, 2017; Argall et al. 2015, 2017, 2018; Aggarwal et al. 2016; Fisher et al. 2016; Smith et al. 2017; Hollick et al. 2018a, 2018b, 2018c; Marchuk et al. 2021). This includes observations of Bernstein waves arising from the PUI population (Joyce et al. 2012).

In this paper, we show examples of the most distant waves with spectral signatures consistent with excitation by newborn interstellar H^+ and He^+ as have been seen by the Voyager 1 spacecraft. These observations from 1991 are the latest high-resolution magnetic field data available to the public for the Voyager mission. We analyze 822 nonoverlapping data intervals and find 80 examples of waves due to pickup H^+. Only 10 examples of waves due to pickup He^+ are shown, but

Original content from this work may be used under the terms of the Creative Commons Attribution 4.0 licence. Any further distribution of this work must maintain attribution to the author(s) and the title of the work, journal citation and DOI.

this is thought to be due to the relatively short duration of most contiguous data intervals making it difficult to get waves at these lower frequencies with good statistical weight.

2. Data Analysis Methods

We analyze each data interval using a combination of prewhitened Blackman–Tukey analyses of the power spectra (Blackman & Tukey 1958; Matthaeus & Goldstein 1982; Chen 1989; Smith et al. 1990; Leamon et al. 1998a, 1998b; Smith et al. 2006a, 2006b; Hamilton et al. 2008; Markovskii et al. 2008, 2015) and FFT analysis of the power and polarization spectra (Fowler et al. 1967; Rankin & Kurtz 1970; Means 1972; Mish et al. 1982). The polarization analysis computes the standard parameters degree of polarization $0 \leqslant D_{\rm pol} \leqslant 1$, coherence $0 \leqslant C_{\rm oh} \leqslant 1$, ellipticity $-1 \leqslant E_{\rm lip} \leqslant 1$, and minimum variance direction $\boldsymbol{k}$. From $\boldsymbol{k}$, we compute the angle between the minimum variance direction and the mean magnetic field $\boldsymbol{B}$ such that $0^\circ \leqslant \Theta_{\rm kB} \leqslant 90^\circ$. These spectra were then examined by eye to find the intervals with wave activity. These are the same techniques used previously to study magnetic waves due to interstellar pickup ions in the ACE, Ulysses, and Voyager data sets (Joyce et al. 2010, 2012; Cannon et al. 2014a; Argall et al. 2015, 2017; Aggarwal et al. 2016; Fisher et al. 2016; Hollick et al. 2018a; Marchuk et al. 2021). Although we have examined the Blackman–Tukey spectra for consistency, we show only the FFT results here. The two are consistent.

Our results presented here are based on the analysis of 822 contiguous intervals of Voyager 1 magnetic field data recorded in 1991. In our earliest analyses of Voyager observations where we searched for evidence of waves due to newborn interstellar pickup ions (PUIs), we undertook a rather hit-or-miss approach of analyzing many intervals of data that seemed like good choices for spectral analysis (Joyce et al. 2010, 2012; Aggarwal et al. 2016). This means nearly stationary flow conditions with a steady mean field and fluctuation level. It is more productive to initiate data selection from automated daily spectrograms of the polarization parameters (Argall et al. 2015, 2017, 2018). This requires that someone examine the plots, find times of strong polarization, and look for evidence of transients that might provide an alternate source of suprathermal ions. These intervals are then analyzed in a manner that allows precise selection of the optimal data intervals (Cannon et al. 2014a; Fisher et al. 2016; Hollick et al. 2018a; Marchuk et al. 2021). That approach is successful—but laborious.

In this analysis, we take advantage of the fact that solar wind conditions at ∼45 au are greatly smoothed relative to 1 au conditions even at solar maximum. This does not mean there are no compression or rarefaction regions, or regions of shear. These things are evident in the Voyager 2 data leading up to this year. It does mean that those transient regions are significantly larger and last longer in the data than transient flows at 1 au and the background magnetic field is very slowly varying. The most significant examples of transient flows at this distance are Merged Interaction Regions (MIRs) and Global Merged Interaction Regions (GMIRs) that we will discuss below. There is one notable GMIR in this year of data.

Voyager 1 magnetic field data at this time come in segments at the highest data rate of one vector every two seconds, with only sparse data available between the segments. This facilitates there being good coverage using hourly data resolution. The high-cadence data are only available in segments that are typically less than eight hours in duration. To take advantage of the segmented and relatively smooth fields, we wrote a data crawler. This code finds the start of any interval of contiguous data, initiates a run file to control the data analysis, and then finds the end of that same data interval. The resulting run file is then used to process the data using a library of routines to produce the results shown here. The result was 823 data intervals studied, with one rejected on the basis of having an unphysical spectrum. We do not know the reason for this single unphysical result, but chose simply to remove it from the analysis as there were more than adequate data to perform the analysis described here. This left 822 data intervals studied and presented here. We did examine the data for shocks as possible alternate sources of the inferred suprathermal ions that act as a source for the reported waves. The data intervals were then passed through a bad point filter to remove measurements more than 2.5 standard deviations from the mean, which is a good indication that the measurement is faulty. The data were padded whenever data were missing (there are short intervals of missing data that are not represented by bad point values in the original data set). The data flagged as bad were interpolated when FFT spectral techniques were used and omitted from the analysis when Blackman–Tukey spectral methods were used. There is very little interpolation required in these data intervals.

3. Data Analysis

Figure 1 shows the mean magnetic field as computed for each of the 822 contiguous intervals of data for Voyager 1 magnetic field measurements in 1991 used in this study. Black circles represent intervals where we do not observe significant evidence of wave activity that can be attributed to pickup H^+. We use these as control intervals to represent the nominal background turbulence. The red triangles represent the wave intervals that appear to arise from pickup H^+. From top to bottom, the figure shows: the mean magnetic field strength B; the mean radial, tangential, and normal components B_R, B_T, and B_N; and the angle between the mean field and radial directions $0^\circ \leqslant \Theta_{\rm BR} \leqslant 90^\circ$. In the ($R$, T, N) heliographic coordinate system, $\hat{\boldsymbol{R}}$ is directed from the Sun to the spacecraft, $\hat{\boldsymbol{T}}$ is coplanar to the Sun's equator and directed in the sense of rotation, and $\hat{\boldsymbol{N}} = \hat{\boldsymbol{R}} \times \hat{\boldsymbol{T}}$. The spacecraft travels from 43.55 au to 47.12 au during this time and remains within a relatively narrow range of heliographic latitude around 31°.5.

As stated above, a characteristic of magnetic field measurements at this time is that they are much smoother than what is commonly seen at 1 au, with steady field conditions lasting for many days. For this reason, the computed means are a good representation of the measurement throughout the interval. There is an exception to this, which can be seen in Figure 1, when a disturbance that occurs shortly after 46 au and the field is intensified. Although the component plots would suggest that the field is redirected at this time, the angle between the mean field and the radial direction is unchanged until the end of the disturbance. This same disturbance was seen by Voyager 2 and studied by Burlaga & Ness (1994), who concluded it was a Merged Interaction Region (MIR). Voyager 1 lacks the thermal ion data to perform that assessment, but the appearance of the same disturbance in the Voyager 1 data suggests it is a Global Merged Interaction Region (GMIR). The distinction between MIR and GMIR only suggests the spatial extent of the object and is not relevant to this study. This disturbance will become

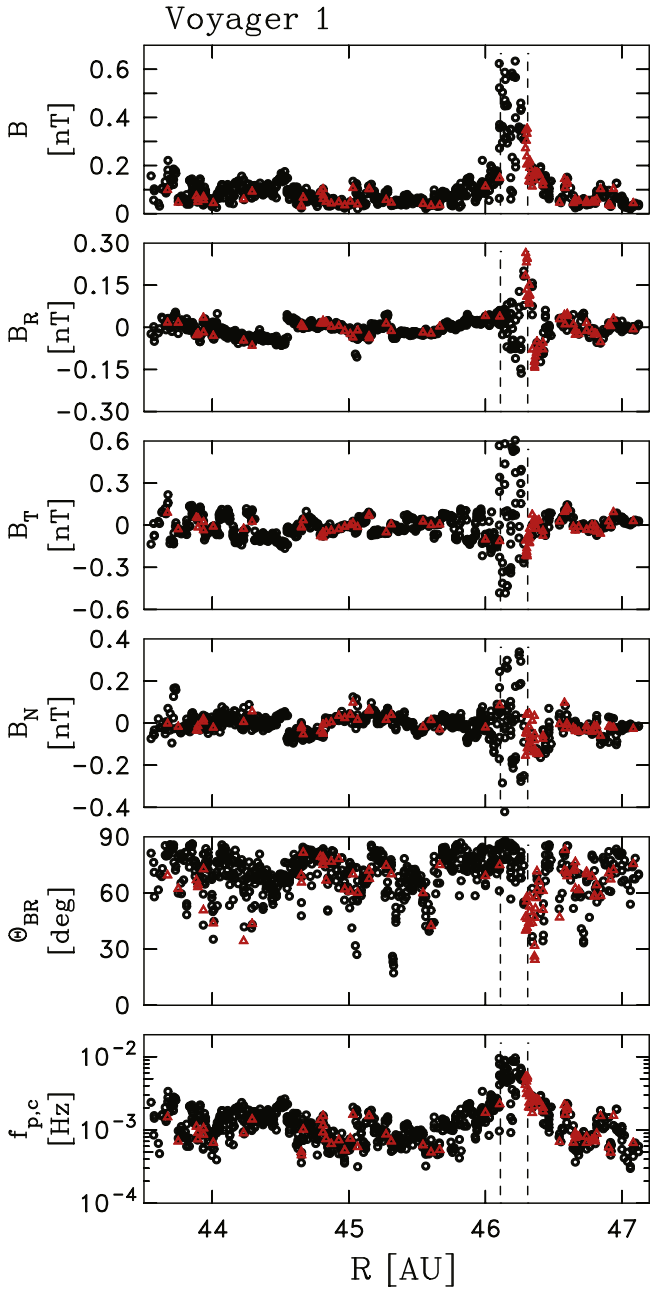

Figure 1. Mean magnetic field parameters for the 822 data intervals used in this study. All are from Voyager 1 measurements recorded during 1991. (top to bottom) Field intensity B; radial, tangential, and normal components B_R, B_T, and B_N; the angle between the mean field and radial directions Θ_{BR}; and the proton cyclotron frequency $f_{p,c}$ as computed from the mean magnetic field. Red triangles represent events showing evidence of wave excitation by pickup H^+. Black circles represent data intervals that do not show evidence of these waves. The vertical dashed lines here and in subsequent figures mark the passage of the GMIR.

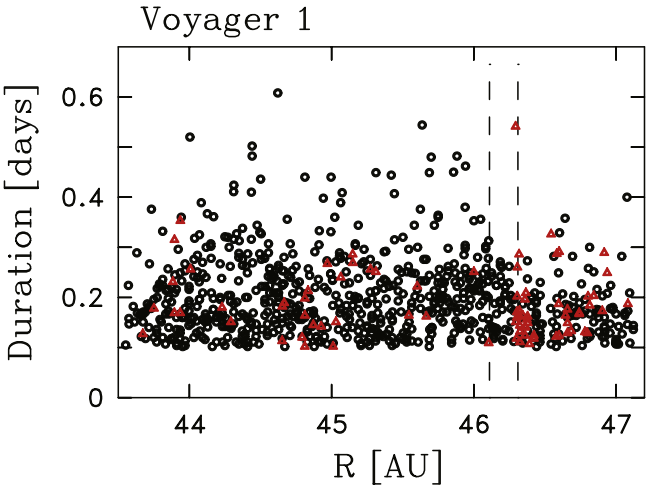

Figure 2. Coverage of the Voyager 1 MAG instrument plotted as fractions of a day for all data intervals recorded in 1991. This represents data availability rather than subsetting performed as part of this analysis. We use whole data intervals as provided (subject to bad point removal) in this analysis, and data intervals can span day boundaries. Red triangles represent events showing evidence of wave excitation by pickup H^+. Black circles represent data intervals that do not show evidence of these waves.

significant in the analysis that follows, as it can be seen that there is a large grouping of wave events following the disturbance. The high-resolution MAG data required to study this same disturbance are not presently available in the online Voyager 2 data.

As described above, we use a data crawler to find segments of contiguous data at 2 s resolution. Figure 2 shows the duration of each data interval obtained in this manner. Intervals of contiguous data tend to span day boundaries, and our analysis does as well. We then perform Blackman–Tukey analyses for the magnetic power spectra (not shown) and FFT analyses of the power and polarization spectra for the 822 contiguous data intervals identified by the data crawler.

We examined every spectrum by eye and by fit to confirm that they met expectations for solar wind spectra. In the process, we examined every power and polarization spectrum for evidence of waves excited by PUIs. This was limited mostly to H^+, but we also searched for waves due to He^+ whenever possible. The short duration of the data intervals negated this search in most instances. Then we ran a code that averages the polarization parameters over the frequency range $f_{p,c} \leqslant f_{sc} \leqslant 2f_{p,c}$ and compared the intervals of $|E_{lip}| > 0.4$ against our earlier list of wave events. We negotiated a compromise between the two lists based on the D_{pol}, C_{oh}, and Θ_{kB} spectra. In the final analysis, the assessment of which data intervals contain strong evidence of waves due to PUIs rests in the combined expectation that D_{pol} and C_{oh} are elevated relative to neighboring frequencies, E_{lip} is biased away from zero, and Θ_{kB} is consistent with quasi-parallel propagation. Not every wave interval displays all of these characteristics to a strong degree, but most do. A few intervals appeared sufficiently compelling in a few characteristics to earn a place on the wave list.

3.1. Waves Due to Pickup H^+

Figure 3 shows three examples of the type of spectra studied here that show evidence of wave excitation by pickup H^+. Each column shows five panels representing the analysis of a single data interval. Top to bottom, they are the diagonal elements of the power spectral density matrix (the power spectrum of the three components of the magnetic field fluctuations) as computed in mean field coordinates, the degree of polarization D_{pol} and coherence C_{oh}, the ellipticity E_{lip}, and the angle between the minimum variance direction and the mean magnetic field Θ_{kB}. A fundamental challenge with the 1991 data is that the contiguous data intervals are relatively short, as shown in Figure 2. In order to obtain statistical weight using

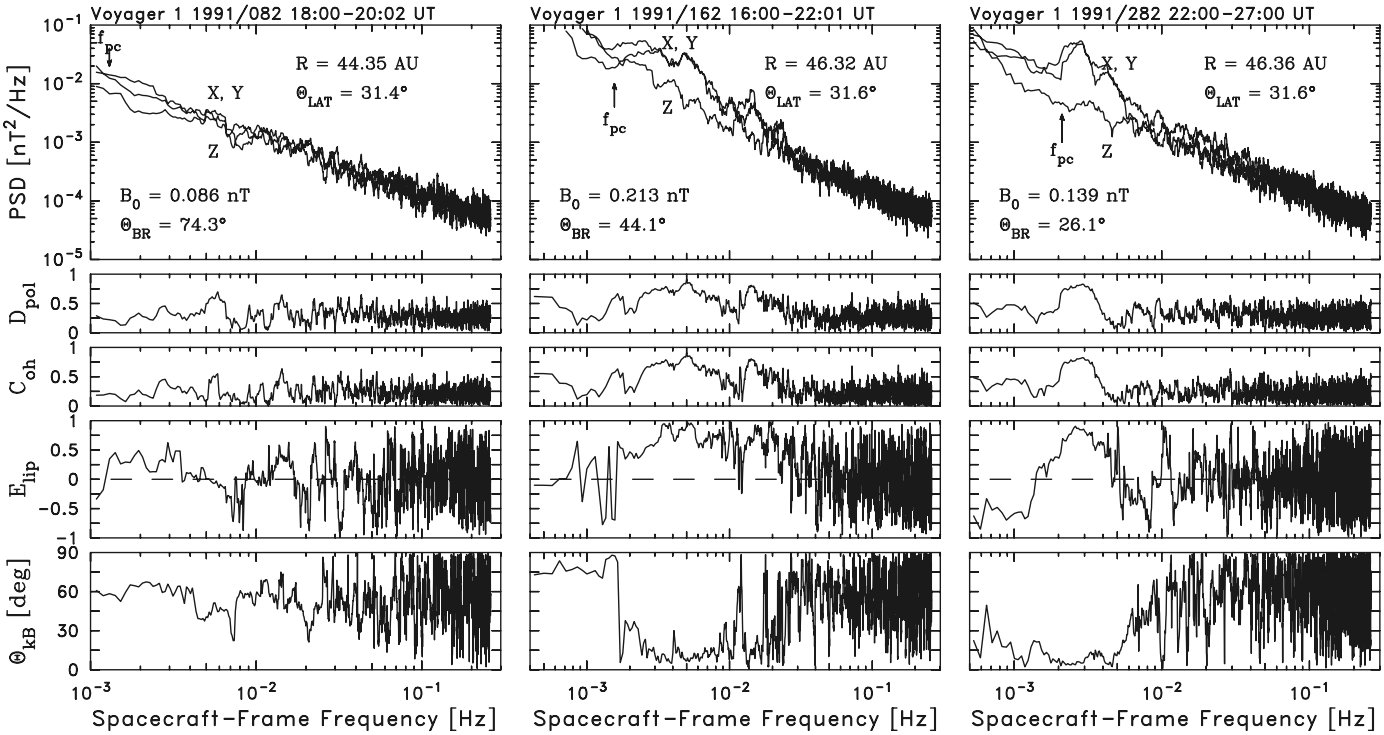

Figure 3. Three examples of the power and polarization spectra studied here. (top to bottom) Power spectral density as computed for the mean field X, Y, and Z components; degree of polarization $0 \leqslant D_{\rm pol} \leqslant 1$; coherence $0 \leqslant C_{\rm oh} \leqslant 1$; ellipticity $-1 \leqslant E_{\rm lip} \leqslant 1$; and angle between the mean magnetic field and minimum variance direction $0^\circ \leqslant \Theta_{\rm kB} \leqslant 90^\circ$. (left) Typical example of a background spectrum without significant evidence for wave excitation. (middle) Typical example of a relatively weak wave spectrum showing excitation by both pickup H^+ and He^+. (right) Textbook example of waves excited by pickup H^+. See text for further discussion.

the FFT methods, the computed spectra must be smoothed. We use an eleven-point sliding boxcar window across the frequencies to smooth the data. This and the short duration of contiguous data intervals sets the minimum frequency that is resolvable as statistically significant at a value that normally resolves $f_{p,c}$ and greater frequencies without the degree of resolution at lower frequencies that is normally desired, but it does not resolve $f_{{\rm He},c}$ in most cases.

Figure 3(left) shows a control spectrum that does not contain waves due to pickup H^+. There is an abundance of publications studying observations from 1 au that report a highly anisotropic background turbulence spectrum. That anisotropy is such that the power associated with the perpendicular fluctuations is greater than the power associated with the parallel fluctuations. However, here we see a nearly isotropic spectrum. An explanation of this is beyond the scope of this paper, but it is not unusual in these observations. There is no enhancement in the magnetic power in the frequency range $f_{p,c} \leqslant f_{\rm sc} \leqslant 2f_{p,c}$, while both $D_{\rm pol}$ and $C_{\rm oh}$ are $\simeq$0.25. There is a bias in $E_{\rm lip} > 0$ that may suggest some excited wave activity, but it is minimal. Finally, the value of $\Theta_{kb} \simeq 60^\circ$. These are not the signatures of waves due to PUIs.

Figure 3(middle) shows an example of a weak wave event that is typical of the wave observations prior to passage of the GMIR. There is a small enhancement in wave power, an increase in $D_{\rm pol}$ and $C_{\rm oh}$, significant bias of $E_{\rm lip} \simeq 0.75$, and $\Theta_{\rm kB} \simeq 10^\circ$. Lee & Ip (1987) predicts left-hand polarized waves in the spacecraft frame ($E_{\rm lip} < 0$). However, in this year and in other Voyager observations beyond $\sim$10 au, there is an abundance of right-hand polarized waves (Hollick et al. 2018a). A smaller percentage is also seen at 1 au (Fisher et al. 2016) and by Ulysses (Cannon et al. 2014a; Marchuk et al. 2021).

Figure 3 (right) shows a near-textbook example of waves excited by pickup H^+. The power spectra show a clear enhancement in power at $f_{\rm sc} > f_{p,c}$ for the two components of the magnetic field fluctuations perpendicular to the mean field. However, the parallel component shows no enhancement. This means that the fluctuations are transverse to the mean magnetic field, as expected. There are strong enhancements at the same frequencies for $D_{\rm pol}$ and $C_{\rm oh}$. There is a strong positive bias in $E_{\rm lip}$ at these same frequencies, indicating right-hand polarization in the spacecraft frame. The expected value of $E_{\rm lip} = -1$ is not seen, but this has become a relatively common observation, as discussed above. In keeping with the transverse nature of the fluctuations, the minimum variance direction is field-aligned. The power spectra return to a nearly isotropic, unpolarized form with $\Theta_{\rm kB} \simeq 90^\circ$ at higher frequencies.

Eighty examples of waves that were most likely excited by newborn pickup H^+ were found. These intervals are listed in Table 1.

Figure 4 shows the power level in the computed trace of the PSD at 10 mHz for each event as determined by a power-law fit to the background spectrum over the frequency range $2 \leqslant f_{\rm sc} \leqslant 30$ mHz that excludes the frequency range $0.8f_{p,c} \leqslant f_{\rm sc} \leqslant 3f_{p,c}$. This is a representation of the background power levels for the measurements that excludes the waves. Two things are notable. First, the power level is remarkably reproducible, except for the region that we conclude marks the passage of the GMIR. Second, the power level does continue to fall slightly with heliodistance, which is an indication that the measured power levels are real and not the result of the ambient field reaching the background noise level of the measurement.

Table 1
Voyager 1 Observations of Waves Due to Pickup H^+ in 1991

Decimal Day	E_{lip}	Decimal Day	E_{lip}	Decimal Day	E_{lip}
013.063–013.190	0.48	022.190–022.368	0.39	034.839–035.070	−0.50
035.148–035.463	0.44	036.834–037.003	0.40	039.137–039.490	−0.55
040.821–040.990	−0.56	047.432–047.688	0.59	069.750–069.930	0.39
076.457–076.608	0.45	111.000–111.113	−0.62	112.443–112.626	0.38
114.317–114.506	0.61	126.257–126.377	0.43	127.259–127.361	0.44
128.332–128.496	−0.36	128.790–128.988	0.40	130.328–130.541	0.37
134.201–134.346	0.38	139.203–139.346	−0.35	144.746–145.012	−0.48
148.399–148.501	−0.35	150.148–150.299	−0.44	153.972–154.212	−0.45
161.159–161.444	0.41	162.681–162.950	0.56	173.679–173.934	0.43
177.668–177.919	0.44	202.414–202.579	0.42	207.610–207.832	−0.56
213.181–213.343	−0.41	248.448–248.699	0.54	256.998–257.107	−0.42
276.408–276.949	0.54	276.952–277.103	0.60	277.366–277.626	0.39
277.641–277.843	−0.09	278.037–278.154	0.67	278.463–278.634	0.76
278.734–278.894	0.64	279.032–279.143	0.82	279.423–279.568	0.52
279.570–279.702	0.82	279.770–279.932	0.80	280.410–280.583	0.43
280.645–280.931	0.51	282.408–282.572	0.54	282.930–283.126	0.70
283.774–283.917	0.66	283.981–284.106	0.61	284.457–284.597	0.82
284.712–284.921	0.50	284.963–285.119	0.53	285.759–285.908	0.50
286.450–286.612	−0.45	286.934–287.041	0.52	289.012–289.130	−0.47
290.186–290.310	−0.24	301.209–301.535	0.66	305.688–305.810	0.41
306.269–306.556	0.39	308.105–308.397	0.60	308.423–308.548	0.69
308.665–308.852	0.52	312.692–312.857	0.55	313.379–313.528	0.57
313.714–313.843	0.53	313.888–314.063	0.54	316.383–316.517	0.52
321.648–321.814	0.58	322.639–322.808	0.11	326.339–326.470	−0.53
327.297–327.499	0.49	328.632–328.761	0.43	329.612–329.797	0.51
331.283–331.487	0.63	337.537–337.710	0.52	340.170–340.459	0.70
341.490–341.739	0.49	356.000–356.187	0.64		

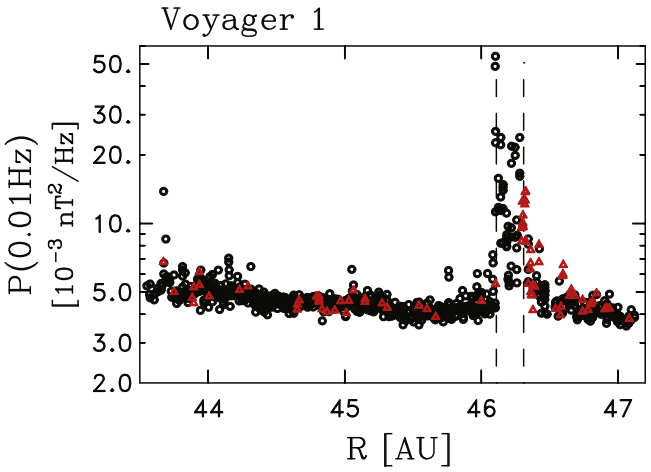

Figure 4. Magnetic power spectral density computed at 10 mHz using the two fit functions. Red triangles and black circles represent wave and control intervals as in Figure 1. Vertical dashed lines again represent the nominal boundaries of the GMIR.

Figure 5(top) shows the peak value of the PSD trace relative to the fit background level in the range $f_{p,c} \leqslant f_{sc} \leqslant 2f_{p,c}$. There are examples of wave spectra, such as those in the middle and right panels of Figure 3, that show enhancements in the power at frequencies attributable to the pickup H^+. However, there are also control intervals where the polarization analyses indicate the absence of waves that show similar enhancements in power. This suggests that most of the enhanced power levels are statistical in nature. We see only a few large enhancements in the power spectrum as a result of newborn interstellar H^+ at these heliodistances.

Figure 5(bottom) shows the frequency where that peak enhancement occurs relative to $f_{p,c}$. Again, this applies to the range $f_{p,c} \leqslant f_{sc} \leqslant 2f_{p,c}$. The peak value occurs across the range of frequencies for both wave intervals and controls with a concentration near $f_{p,c}$. This concentration near $f_{p,c}$ is in keeping with the theory of wave excitation by newborn interstellar PUIs (Lee & Ip 1987), but it applies equally well to the control intervals. This lends further support to the claim that most of the wave power signatures are nothing more than statistical fluctuations of the background spectrum.

Figure 6 shows our analysis of the polarization parameters averaged over the frequency range $f_{p,c} \leqslant f_{sc} \leqslant 2f_{p,c}$. Here, we focus on waves with properties that indicate excitation by pickup H^+; we will discuss the He^+ source later. Figure 6(top) plots the degree of polarization as a function of the ellipticity. This shows what we have seen before with Voyager observations (Hollick et al. 2018a). Here, the results appear more scattered, but the organization of wave and background events remains. There is a central accumulation of results with $-0.4 \leqslant E_{lip} \leqslant 0.4$ that represents background intervals without evidence of enhanced wave activity. With three exceptions, the wave intervals display $|E_{lip}| > 0.4$. Those exceptions were chosen because they had enhancements in E_{lip} at marginally higher frequencies that were judged to likely be the result of pickup H^+, but they form a very small minority of observations. Wave polarizations in the spacecraft frame are expected to be left-handed ($E_{lip} < 0$) due to a dominance of right-hand polarized, sunward-propagating waves in the plasma frame (Lee & Ip 1987). However, a majority of right-hand polarized observations in the spacecraft frame have been reported for Voyager observations beyond ∼10 au (Hollick et al. 2018a). Here, we see a strong dominance of right-handed waves. We do not have an explanation of this result at this time.

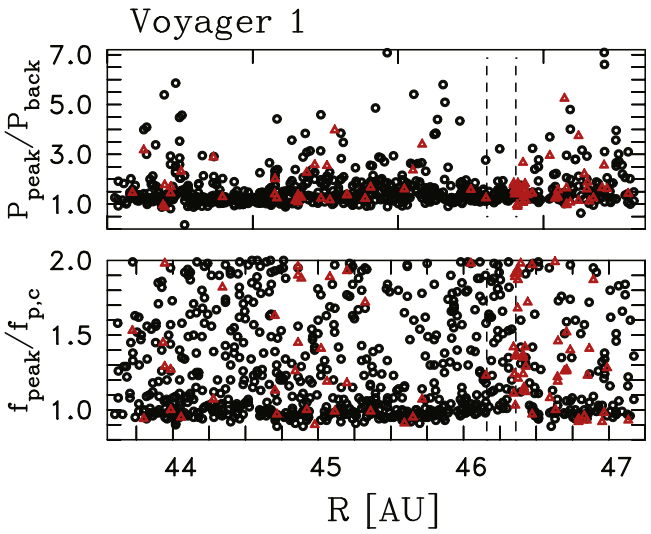

Figure 5. (top) Peak power enhancement in the trace of the PSD relative to the background level. (bottom) Frequency relative to $f_{p,c}$ where the peak power enhancement occurs. Vertical dashed lines again represent the nominal boundaries of the GMIR.

As $|E_{\rm lip}|$ increases with the wave observations, $D_{\rm pol}$ tends to increase as well. This is expected because waves tend to exhibit greater degrees of polarization than turbulence. However, it is clear that this is not always the case.

The second panel of Figure 6 plots the coherence as a function of the degree of polarization. Both the background and wave results follow previous expectations (Hollick et al. 2018a; Marchuk et al. 2021). Wave observations follow a confined linear relationship $C_{\rm oh} \simeq D_{\rm pol}$, while the turbulence intervals show $C_{\rm oh} \leqslant D_{\rm pol}$.

The third panel of Figure 6 plots the ellipticity as a function of heliodistance R. While it is evident that the wave intervals are seen throughout the year, there is an abundance of events with large values of $E_{\rm lip}$ immediately following the GMIR that continue throughout the remainder of the year. Thermal ion data from the PLS instrument (Bridge et al. 1977) are not available at this time, as the instrument failed shortly after encounter with Saturn. Therefore, we lack wind speed, density, and thermal proton temperature in this analysis. Because of this, we are unable to calculate meaningful estimates of the turbulence rate using in situ data, while the ionization rate and wave growth rate can only be approximated by expected flow conditions. It has been shown that, while theory indicates waves are continuously excited by newborn interstellar PUIs, they are only seen when the rate of wave energy excitation exceeds the rate that turbulence reprocesses the energy within the spectrum (Cannon et al. 2014b; Aggarwal et al. 2016; Fisher et al. 2016; Hollick et al. 2018b; Marchuk et al. 2021). We are unable to perform those calculations here, so we are unable to determine whether the waves are seen because the ionization rate increases or the turbulence rate decreases.

The bottom panel of Figure 6 plots the angle between the minimum variance and mean field directions as a function of heliodistance. That angle, which is often described as the propagation direction for low-frequency waves, is widely scattered across the full range of possibilities with a concentration near $\Theta_{\rm kB} \simeq 90°$. This concentration might be indicative of two-dimensional turbulence. The wave intervals show $\Theta_{\rm kB}$ scattered over the full range of possible values, but

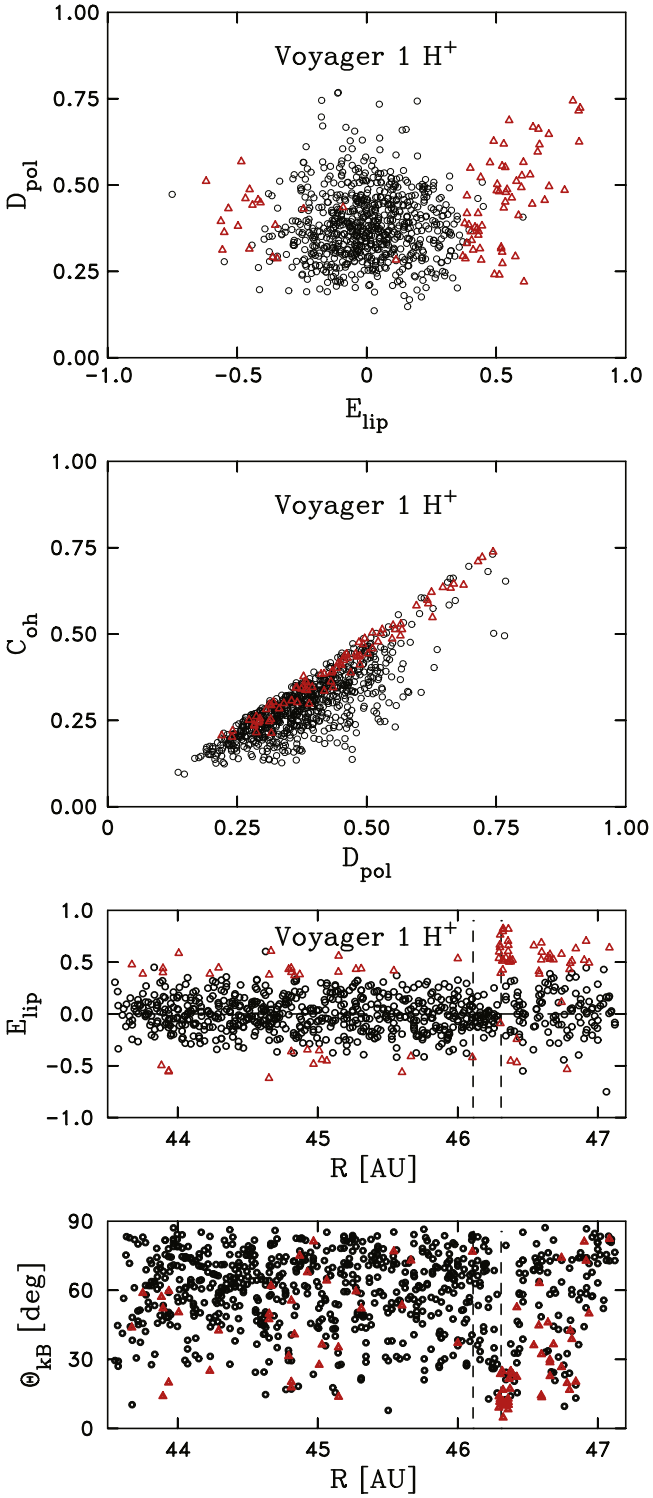

Figure 6. Coherence $C_{\rm oh}$, degree of polarization $D_{\rm pol}$, ellipticity $E_{\rm lip}$, and angle between the mean field and minimum variance directions $0° \leqslant \Theta_{\rm kB} \leqslant 90°$, plotted to show their general relationships and locations within the year of data. Red triangles and black circles represent wave and control intervals as in Figure 1. This convention continues throughout the paper.

the particularly intense events at the trailing edge of the GMIR show $\Theta_{\rm BR} < 30°$.

The Lee & Ip (1987) theory assumes a radial mean magnetic field, although this is not expected to be a severe limitation of the theory unless the mean field is very close to azimuthal, which can alter the resonance condition. Past studies have

Table 2
Voyager 1 Observations of Waves Due to Pickup He^+ in 1991

Decimal Day	E_{lip}	Decimal Day	E_{lip}	Decimal Day	E_{lip}
039.137–039.490	−0.92	162.681–162.950	0.49	254.870–254.986	0.43
276.408–276.949	0.11	276.952–277.103	−0.16	279.032–279.143	0.31
284.712–284.921	−0.39	285.759–285.908	−0.28	308.105–308.397	0.65
308.665–308.852	0.61				

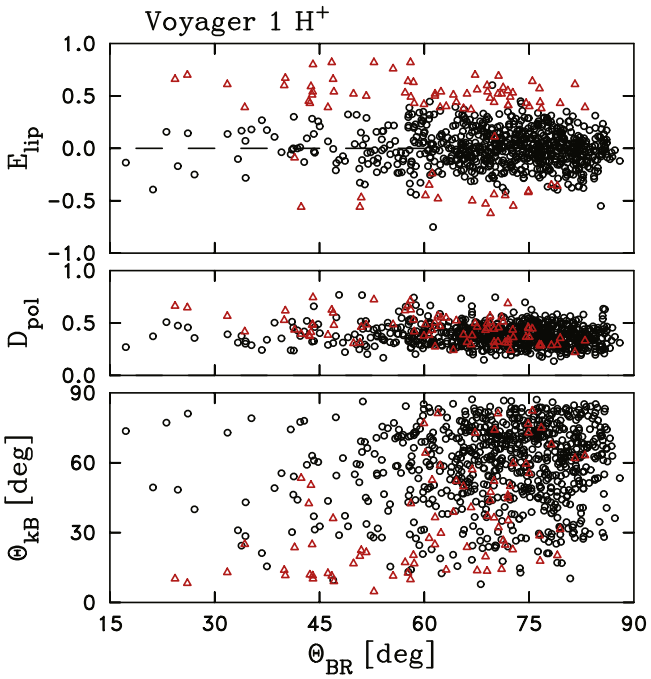

Figure 7. Red triangles and black circles represent wave and control intervals as in Figure 1. (top) Ellipticity E_{lip} plotted as a function of the angle between the mean magnetic field and the radial direction Θ_{BR}. There is no clear enhanced likelihood of observing strong wave signatures when the mean magnetic field has any particular orientation, including radial. (middle) Degree of polarization D_{pol} plotted as a function of the angle between the mean magnetic field and the radial direction Θ_{BR}. There is very little that distinguishes D_{pol} for wave events. (bottom) The angle between the minimum variance direction and the mean magnetic field Θ_{kB} plotted as a function of the angle between the mean magnetic field and the radial direction Θ_{BR}. Although there is a tendency for the minimum variance direction to be more nearly field-aligned for wave events than for controls, the observed angles cover the full range of possible values.

shown that waves tend to be observed when the turbulence level is low (Cannon et al. 2014b; Aggarwal et al. 2016; Fisher et al. 2016; Hollick et al. 2018b; Marchuk et al. 2021), which includes rarefaction regions. The absence of thermal ion data at this time prevents our direct examination of the wave growth rates, the turbulence rates, or the flow conditions. This includes the type of rarefaction region that is threaded by a radial magnetic field. Figure 7 (top) plots the ellipticity E_{lip} as a function of the angle between the mean magnetic field and the radial direction Θ_{BR} where black circles represent control intervals and red triangles represent wave observations. There is no evidence that waves are observed for any limited range of Θ_{BR}. However, it is also true that the data in 1991 avoid the orientations $0° < \Theta_{BR} < 15°$. This suggests that the instability is active throughout the observed range of Θ_{BR}.

Figure 7(middle) plots the degree of polarization D_{pol} as a function of Θ_{BR}. There is very little distinction in D_{pol} between waves and control intervals. Ideally, the wave intervals would show $D_{pol} \simeq 1$, but these are largely marginal events with very weak growth rates that must accumulate energy over long periods of time. The dependence of the coherence C_{oh} upon Θ_{BR} is largely identical to D_{pol} and is not shown. It appears that the spectrum can accumulate E_{lip} more readily than it strengthens D_{pol} or C_{oh}.

Figure 7 (bottom) plots the angle between the minimum variance direction and mean magnetic field Θ_{kB} as a function of Θ_{BR}. While it is true that Θ_{kB} varies over the full range of possible values, there is a significant number of wave events with $\Theta_{kB} < 30°$ when $\Theta_{BR} < 60°$. However, when $\Theta_{BR} > 60°$, the minimum variance direction trends away from being field-aligned.

3.2. Waves Due to Pickup He^+

As stated above, most available data intervals are too short to obtain statistically significant estimates for the spectra at the He^+ cyclotron frequency $f_{He,c}$. However, we did find ten instances where we believe we can reliably state that waves due to pickup He^+ are resolved. These intervals are listed in Table 2.

Figure 8 shows spectra from three of these events where $f_{He,c} = f_{p,c}/4$. Figure 8(left) shows an example from before passage of the GMIR where the frequencies $f_{He,c} \leqslant f_{sc} \leqslant 2f_{He,c}$ are well resolved. There is no evidence of enhanced power due to either pickup He^+ or H^+, which is a common feature for waves due to newborn interstellar pickup He^+ in the Voyager data in the outer heliosphere (Hollick et al. 2018a). D_{pol} and C_{oh} show only small enhancements at He^+ frequencies, but E_{lip} shows a large enhancement at pickup He^+ frequencies that is distinct from the enhancement at H^+ frequencies. Both are positive, which is not the textbook example for these waves, but it is a common feature as stated above. For both He^+- and H^+-excited waves, the minimum variance direction is field-aligned.

Figure 8 (middle) shows an example of waves with properties indicating excitation by pickup He^+ that occurs at the end of the GMIR. There is arguably a minor enhancement in the power due to H^+, but not due to He^+. Both D_{pol} and C_{oh} show clear and significant enhancements at He^+ frequencies. The interesting thing about this example is that E_{lip} for the waves due to He^+ has the opposite polarization (left-handed) when compared to the waves due to pickup H^+ (right-handed), thereby indicating that the sources are very likely independent. Both He^+ and H^+ waves have minimum variance directions that are field-aligned.

Figure 8 (right) shows an example that is similar to the left panel that occurs after passage of the GMIR. D_{pol} and C_{oh} both show minor enhancements at He^+ frequencies. E_{lip} shows two strong, separated features indicating right-hand polarized waves at both He^+ and H^+ frequencies. Both sets of waves have minimum variance directions that are field-aligned.

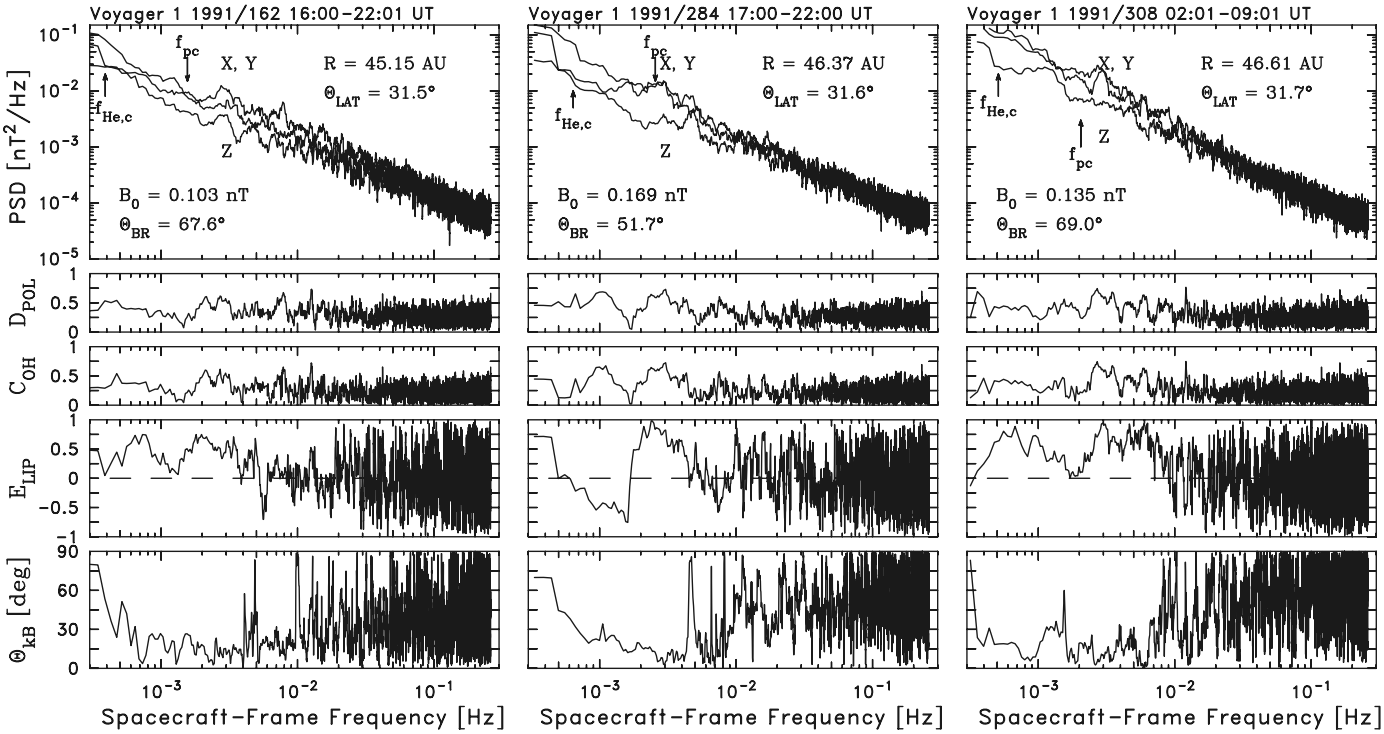

Figure 8. Three examples of the power and polarization spectra studied here that show evidence of wave excitation by pickup He^+. Same format as Figure 3. See text for further discussion.

As there are relatively few examples of waves due to pickup He^+, we omit much of the analysis described above for waves due to H^+. The examples shown in Figure 8 are good representations of the observations. We strongly suspect that waves due to pickup He^+ would be seen more often if the contiguous data intervals were longer in duration. At the same time, the production rate for interstellar PUIs decreases with heliocentric distance more strongly for He^+ than for H^+ (Hollick et al. 2018b; Sokół et al. 2019). The difference in the production rate is almost two orders of magnitude at these distances. This is because the density of interstellar He is smaller than the density of interstellar H beyond the density depletion region (i.e., ionization cavity) and at distances greater than about 5–10 au in the upwind direction. Because the number density of pickup He^+ is falling more rapidly than H^+ and resonates at lower spacecraft frequencies where the ambient power level is higher than for H^+, the likelihood that there are unresolved waves excited by pickup He^+ is limited and unlikely to exceed the number events due to H^+.

4. Discussion

The PLS instrument on Voyager 1 died shortly after the Saturn encounter, leaving the spacecraft without thermal ion data. No wind speed or proton density data are available to support the MAG data used here. This makes it difficult to provide the newborn PUI rates, the wave excitation rates, and the turbulence rates. In past studies, it has been argued that wave excitation is ongoing at a rate that varies with the ionization rate, which itself depends mostly on collisions with either solar EUV photons in the case of He^+ production or solar wind thermal proton collisions in the case of H^+. Waves are seen when the wave excitation rate exceeds the rate at which turbulence remakes the energy as part of the spectral transport that heats the background plasma (Cannon et al. 2014b; Aggarwal et al. 2016; Fisher et al. 2016; Hollick et al. 2018b; Marchuk et al. 2021). While we are unable to estimate the turbulence rates from the observations, the magnetic power level at the relevant spacecraft-frame frequencies is a significant contributor to the calculation. Figure 4 does not show significant depletion of the background power level during the reported wave events. This leaves us to question whether the ionization rates are increased when the waves are seen.

An interesting feature of this paper, in addition to revealing the most distant examples of waves consistent with excitation by newborn interstellar pickup ions, is the fact that there is a clustering of the strongest events at the trailing edge of a GMIR that passes over the spacecraft. The measured mean magnetic field shows enhanced intensity associated with the GMIR while the orientation undergoes relatively little change. This leads us to question whether an extended rarefaction region follows the GMIR, and since rarefaction regions tend to show reduced turbulence levels, it is thought that this may provide at least a partial explanation for the observation of the strongest wave events following the GMIR.

In an attempt to address this and related possibilities, we have applied the Sun Heliosphere Observation-based Ionization Rates (SHOIR) model (Sokół et al. 2020) to calculate production rates for interstellar PUIs, following the methodology applied in Hollick et al. (2018b). While this analysis indicates up to a factor of four increase in H^+ production, it is mostly associated with the flow a few days after the passage of an apparent shock at the leading edge of the GMIR. That apparent shock occurred within a magnetic field data gap and without PLS data to substantiate the identification. Due to limited resolution time, this model is not able to explain the

clustering of strong events over forty days following the GMIR. However, the calculations do show an ongoing increase in the production rates for H^+ in the first half of 1991. This is due to an elevated solar wind density during that time, which relates to the solar wind dynamic pressure enhancement observed in that period (Sokół et al. 2021). For comparison, we applied the same model to the Voyager 2 observations in 1991 using plasma data with their available time resolution. There, we find smaller enhancements in the ion production. Voyager 2 also shows brief periods of reduced solar wind density following the GMIR that could double the rate of wave excitation for the same ion production rate, but they last for only a partial day. Much longer rarefactions would be needed to explain the Voyager 1 observations.

Apart from passage of the GMIR, the Voyager 1 spacecraft has entered a range within the outer heliosphere where both the turbulence level and the wave excitation rate tend to become approximately constant or slowly varying with heliocentric distance. It is therefore thought that the observations shown here are likely to be representative of what might be seen at greater heliocentric distances, should those data become available and to whatever extent the instrument noise does not overwhelm the wave signal.

5. Summary

We have shown our analysis of magnetic waves that we contend are excited by newborn interstellar pickup H^+ and He^+ as found by the Voyager 1 MAG instrument in 1991 when the spacecraft traveled from 43.55 to 47.12 au at 31° north latitude. The waves excited by H^+ are relatively abundant, with 80 examples out of the 822 data intervals studied. Observations of waves excited by He^+ are less abundant, but the relatively short duration of contiguous data intervals makes it difficult to resolve He^+ cyclotron frequencies with adequate statistical weight to make reliable determinations. The passage of a GMIR late in the year plays a prominent role in the excitation of the waves, although exactly how it achieves this is not determined. Waves that are right-hand polarized in the spacecraft frame continue to play a major role in the analysis despite the fact that theory predicts the observations should be left-hand polarized. We do not have an explanation for this, although it is seen in numerous other studies using the ACE, Ulysses, and Voyager spacecraft data.

Past studies where thermal ion data are available have shown that waves due to newborn interstellar pickup ions are seen when the turbulence is sufficiently weak to allow for the slow growth of the waves (Cannon et al. 2014b; Aggarwal et al. 2016; Fisher et al. 2016; Smith et al. 2017; Hollick et al. 2018b; Marchuk et al. 2021). Those data and the required analysis are not available for Voyager 1 in 1991. However, it is clear from the analysis here that the times of low turbulence levels required for the ever-present instability to achieve observable wave levels continue at this distance. The implication is that the ionization rates and resulting wave growth rates that continue to fall with increasing heliospheric distance are a good match for the falling turbulence levels. This results in the ongoing ability to observe these waves in the outer heliosphere.

C.W.S., P.A.I., S.H., and Z.B.P. are supported by NASA grant NNX17AB86G. B.J.V. is supported by NSF grant AGS1357893. B.J.V. and P.A.I. are supported under NASA HSR grant 80NSSC18K1215. C.J.J. and N.A.S. are supported by the Interstellar Boundary Explorer mission as a part of NASA's Explorer Program, partially by NASA SR&T Grant NNG06GD55G, and by the Sun-2-Ice (NSF grant number AGS1135432) project. C.W.S., B.J.V., P.A.I., and N.A.S. were partially supported by NASA grant 80NSSC17K0009. This work was performed while L.A.E. was a student at Contoocook Valley Regional High School in Peterborough, New Hampshire. J.M.S. is partially supported by IBEX grant 80NSSC20K0719 and NASA grant 18-DRIVE18_2-0029, Our Heliospheric Shield, 80NSSC22M0164. L.F.B. is supported by NASA contract 80GSFC19C0012. We thank A. Szabo and J. Park of GSFC for checking the instrument calibration to confirm the GMIR. The data used in this analysis are available from the NSSDC.

ORCID iDs

Charles W. Smith https://orcid.org/0000-0002-5379-1542
Matthew R. Argall https://orcid.org/0000-0001-6315-1613
Colin J. Joyce https://orcid.org/0000-0002-3841-5020
Philip A. Isenberg https://orcid.org/0000-0003-0505-8546
Bernard J. Vasquez https://orcid.org/0000-0001-8593-7289
Nathan A. Schwadron https://orcid.org/0000-0002-3737-9283
Justyna M. Sokół https://orcid.org/0000-0002-4173-3601
Leonard F. Burlaga https://orcid.org/0000-0002-5569-1553

References

Aggarwal, P., Taylor, D. K., Smith, C. W., et al. 2016, ApJ, 822, 94
Argall, M. R., Fisher, M. F., Joyce, C. J., et al. 2015, GeoRL, 42, 9617
Argall, M. R., Hollick, S. J., Pine, Z. B., et al. 2017, ApJ, 849, 61
Argall, M. R., Hollick, S. J., Pine, Z. B., et al. 2018, ApJ, 854, 77
Blackman, R. B., & Tukey, J. W. 1958, The Measurement of Power Spectra (Mineola, NY: Dover)
Bridge, H. S., Belcher, J. W., Butler, R. J., et al. 1977, SSRv, 21, 259
Burlaga, L. F., & Ness, N. F. 1994, JGR, 99, 19341
Cannon, B. E., Smith, C. W., Isenberg, P. A., et al. 2013, in AIP Conf. Proc. 1539, Solar Wind 13, ed. G. P. Zank et al. (Melville, NY: AIP), 334
Cannon, B. E., Smith, C. W., Isenberg, P. A., et al. 2014a, ApJ, 784, 150
Cannon, B. E., Smith, C. W., Isenberg, P. A., et al. 2014b, ApJ, 787, 133
Cannon, B. E., Smith, C. W., Isenberg, P. A., et al. 2017, ApJ, 840, 13
Chen, J. 1989, PhD thesis, Univ. of Del., Newark
Fisher, M. K., Argall, M. R., Joyce, C. J., et al. 2016, ApJ, 830, 47
Fowler, R. A., Kotick, B. J., & Elliott, R. D. 1967, JGR, 72, 2871
Hamilton, K., Smith, C. W., Vasquez, B. J., & Leamon, R. J. 2008, JGR, 113, A01106
Hollick, S. J., Smith, C. W., Pine, Z. B., et al. 2018a, ApJ, 863, 75
Hollick, S. J., Smith, C. W., Pine, Z. B., et al. 2018b, ApJ, 863, 76
Hollick, S. J., Smith, C. W., Pine, Z. B., et al. 2018c, ApJS, 237, 34
Hollick, S. J., Smith, C. W., Pine, Z. B., et al. 2022, JGRA, 127, e30086
Joyce, C. J., Smith, C. W., Isenberg, P. A., et al. 2012, ApJ, 745, 112
Joyce, C. J., Smith, C. W., Isenberg, P. A., Murphy, N., & Schwadron, N. A. 2010, ApJ, 724, 1256
Leamon, R. J., Smith, C. W., & Ness, N. F. 1998b, GeoRL, 25, 2505
Leamon, R. J., Smith, C. W., Ness, N. F., Matthaeus, W. H., & Wong, H. K. 1998a, JGR, 103, 4775
Lee, M. A., & Ip, W.-H. 1987, JGR, 92, 11041
Marchuk, A. V., Smith, C. W., Watson, A. S., et al. 2021, ApJ, 923, 185
Markovskii, S. A., Vasquez, B. J., & Smith, C. W. 2008, ApJ, 675, 1576
Markovskii, S. A., Vasquez, B. J., & Smith, C. W. 2015, ApJ, 806, 78
Matthaeus, W. H., & Goldstein, M. L. 1982, JGR, 87, 6011
Means, J. D. 1972, JGR, 77, 5551
Mish, W. H., Wenger, R. M., Behannon, K. W., & Byrnes, J. B. 1982, Interactive Digital Signal Processor, NASA Technical Memorandum (Revised 1984), 83997, Goddard Space Flight Center, Greenbelt, MD, https://ntrs.nasa.gov/citations/19840026903

Murphy, N., Smith, E. J., Tsurutani, B. T., Balogh, A., & Southwood, D. J. 1995, SSRv, 72, 447
Rankin, D., & Kurtz, R. 1970, JGR, 75, 5444
Smith, C. W., Aggarwal, P., Argall, M. R., et al. 2017, JPhCS, 900, 012018
Smith, C. W., Hamilton, K., Vasquez, B. J., & Leamon, R. J. 2006a, ApJL, 645, L85
Smith, C. W., Matthaeus, W. H., & Ness, N. F. 1990, Proc. ICRC (Adelaide), 5, 280
Smith, C. W., Vasquez, B. J., & Hamilton, K. 2006b, JGR, 111, A09111
Sokół, J. M., Dayeh, M. A., Fuselier1, S. A., et al. 2021, ApJ, 922, 250
Sokół, J. M., Kubiak, M. A., & Bzowski, M. 2019, ApJ, 879, 24
Sokół, J. M., McComas, D. J., Bzowski, M., & Tokumaru, M. 2020, ApJ, 897, 179